
Title: Enhanced photocatalytic performance of zinc oxide nanostructures via photoirradiation hybridisation with graphene oxide for the degradation of triclosan under visible light: Synthesis, characterisation and mechanistic study

Authors: Nancy Cervantes Rincón, Samia Ben Hammouda, Mika Sillanpää, Vladimir Escobar Barrios

PII: S2213-3437(18)30608-0
DOI: https://doi.org/10.1016/j.jece.2018.09.064
Reference: JECE 2685

To appear in:

Received date: 26-6-2018
Revised date: 27-9-2018
Accepted date: 29-9-2018

Please cite this article as: Rincón NC, Hammouda SB, Sillanpää M, Barrios VE, Enhanced photocatalytic performance of zinc oxide nanostructures via photoirradiation hybridisation with graphene oxide for the degradation of triclosan under visible light: Synthesis, characterisation and mechanistic study, *Journal of Environmental Chemical Engineering* (2018), https://doi.org/10.1016/j.jece.2018.09.064

**Enhanced photocatalytic performance of zinc oxide nanostructures via photoirradiation hybridisation with graphene oxide for the degradation of triclosan under visible light: Synthesis, characterisation and mechanistic study**

Nancy Cervantes Rincón[1,2], Samia Ben Hammouda[2], Mika Sillanpää[2], Vladimir Escobar Barrios[1*]

[1]*C.P. 78216, San Luis Potosí, S.L.P., México*

[2]*Laboratotory of Green Chemistry, School of Engineering Science, Lappeenranta University of Technology, Sammonkatu 12, Fi-50130 Mikkeli, Finland*

[*]Corresponding author: vladimir.escobar@ipicyt.edu.mx

Graphical Abstract

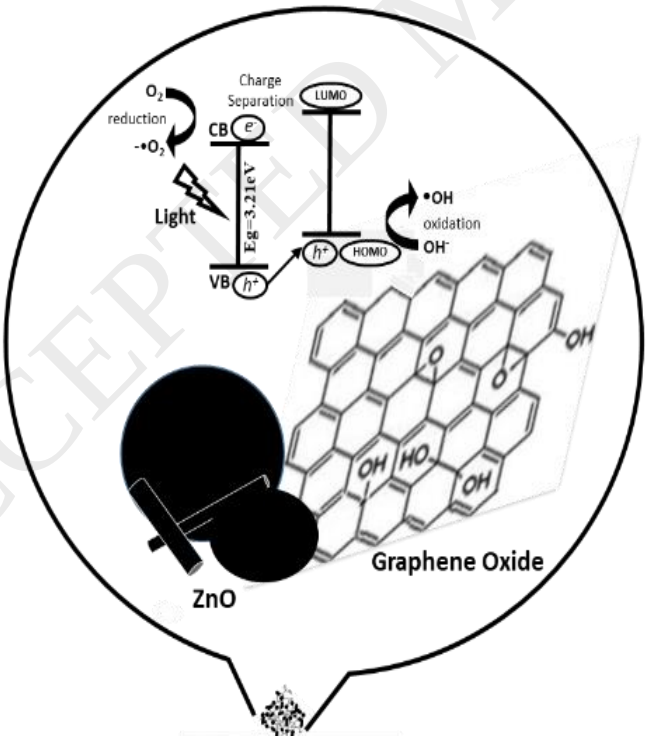

# Highlights

- Modification of ZnO with graphene oxide (GO) gives a highly effective photocatalyst able to carry out photodegradation of Triclosan.
- The photoirradation method gives high effective ZnO/GO hybrid photocatalyst for triclosan degradation. In addition, such synthesis method is a cheap and very quickly way to generate low GO content photocatalyst, which has comparable performance to other photocatalyst that have higher OG content.
- It was established that OG acts like an electron trap enhancing the photocatalytic performance.
- The ZnO/GO photocatalyst is able to degrade Triclosan under visible light up to 47 % of the initial concentration.

**ABSTRACT**

Modification of ZnO nanoparticles with graphene oxide (GO) was carried out, and the obtained hybrid photocatalyst was used for the photodegradation of triclosan (TCS), which is an endocrine disrupting compound. Three different concentrations of GO were used to modify ZnO catalyst using the photoirradiation method and the resultant materials were characterised by SEM, TEM, Zeta Potential, FTIR, Raman, $N_2$ Physisorption, HPLC, XRD and UV-Vis spectrophotometry in order to determine their physico-chemical and photocatalytic properties. Regarding the photocatalytic evaluation, the results of the photodegradation process for TCS showed that GO acts as a trap of electrons improving the performance of ZnO even at low TCS concentration (8 $mg.L^{-1}$) under visible light radiation. The GO-modified composite that contains the highest GO concentration (0.5% w/w) was the material that showed the best photocatalytic performance under visible light degrading up to 45% of the initial concentration of TCS and showed a reaction rate constant two times higher than pristine zinc oxide. This study allowed us to propose the photocatalytic mechanism of ZnO/GO hybrid photocatalysts to degrade TCS. In addition, this research contributes to the understanding of the enhancement of the efficiency of ZnO/GO hybrids and contributes to obtaining a photoactive material with promising use under natural light radiation in an Advance Oxidation Process to eliminate endocrine-disrupting compounds such as triclosan.

**KEYWORDS**

Nano-ZnO/GO photocatalysts, triclosan, UV light, visible light, photocatalysis

## 1. INTRODUCTION

In recent years, a growing problem with water treatment has arisen due to the presence of endocrine disrupting compounds (EDC), which persist in surface, waste, and drinking water. The term endocrine disrupting compounds defines a diverse and heterogeneous group of chemicals that can alter hormonal balance [1], which means that they interfere in the normal functions of the hormonal processes of living beings. Such chemical compounds can mimic hormones, due to their similar chemical structure, but they do not act as hormones and are responsible for the homeostasis, reproduction, and developmental process in living beings [2,3]. The ways to exposure with EDCs occurs through drinking contaminated water, breathing contaminated air, ingesting food, or coming into contact with contaminated soil.

A significant example of EDC is triclosan (TCS), a bactericidal widely used in deodorant formulations, toothpastes, soaps, powders, cosmetics, textiles, plastics, polymers, fibres, and medical implant devices. Then, given the use of these products, triclosan has been directly discharged into wastewater, although it has also been detected in surface water, sludge, sediment, and drinking water, and several studies have reported its presence in waters and wastewaters in the US and Europe at a very low concentration in the range of $ng.L^{-1}$. Moreover, it has been stated that when irradiated by UV light, triclosan (in its anionic form) is involved in an efficient ring closure. It leads to the formation of highly toxic compounds like chlorodioxins [4].

The treatment of water, by conventional methods, removes in some cases up to 90% of EDC. However, with such residual concentrations of triclosan it is necessary to develop methods to remove even trace concentrations of these pollutants.

Advanced Oxidation Processes (AOPs) is one of the most effective method due to the high oxidising power of free radicals generated during such processes, like hydroxyl radical ($^{\bullet}OH$), which is able to mineralise compounds that cannot be oxidised by oxidising agents such as oxygen, ozone, and chlorine [4].

Among the methodologies to generate hydroxyl free radicals, we can find the heterogeneous photocatalysis, which is usually carried out under ultraviolet radiation in order to activate the semiconductor and thereby to trigger reduction and oxidation reactions that are responsible for degrading and mineralising organic compounds, such as triclosan.

Generally, the semiconductors used for this purpose are cheap, non-toxic, and can be regenerated without losing their photocatalytic activity [5, 6]. Examples of the most used semiconductors in heterogeneous photocatalysis for organic compounds are titanium dioxide, zinc oxide, tellurium cadmium, and zinc selenide, although the titanium dioxide is the material that has gained much attention and we can find extensive literature regarding this compound.

However, in the case of $TiO_2$, its oxidative degradation, by the effect of a high recombination of electrons, limits its use at industrial scale. On the other hand, ZnO has attracted much attention in the degradation of various pollutants due to its high photosensitivity. The ZnO has wide band gap (3.37 eV), large excitation binding energy (60 MeV) and low threshold power for optical pumping and is thus considered a low cost alternative photocatalyst to $TiO_2$ for the degradation of organic compounds in aqueous solution [7, 8].

In addition, ZnO absorbs a greater fraction of the radiation spectrum for the photocatalytic process and, therefore, it has been used in the manufacture of solar panels and for opto-electronic applications. This characteristic of ZnO to absorb a larger fraction of the radiation spectrum and its chemical resistance opens the possibility to use this material in water treatment to degrade EDC, such as triclosan.

The photodegradation of triclosan, until complete mineralisation, has been studied in hybrid systems, especially binary ones, such as $TiO_2$/UV [9]. Despite the advantages of ZnO and its promising application in photocatalytic degradation using sunlight, there are questions to be answered regarding the degradation of EDC, such as triclosan, because the main problem that affects the photocatalytic efficiency of semiconductors as ZnO is the recombination of excited electrons, which decreases the formation of hydroxyl free radicals and, hence, there is a decrement of the efficiency of pollutant degradation. Thus, some strategies have been focused to reduce the recombination of excited electrons, such as the modification of ZnO nanoparticles with metal, thereby forming hetero-structure. The obtained results by other researchers show the relevance of modifying the ZnO with gold [10], silver [11] and platinum [12] nanoparticles for the photodegradation of different organic pollutants as dyes [13,14], considering that they are good electron conductors, property that imparts to the ZnO a delayed recombination of excited electrons.

However, metals are not the only materials that exhibit good electrical properties to retard the electron recombination process occurring in photocatalysts. Recently, graphene oxide (GO) has been used for the development of new materials by its incorporation in polymeric matrices, due to its chemical surface properties (functional groups), which promote the interactions between GO and polymer [15].

Furthermore, the graphene oxide may exceed the electron transport property, a key characteristic of metals, depending on the amount of functional groups present on its surface [16]. Studies show excellent chemical properties of GO to form compounds with other materials due to its surface chemistry as well as having the ability to be

reduced to graphene using ultraviolet radiation [17]. Thus, it is possible to obtain compounds of ZnO/GO or ZnO/Graphene with high thermal and electrical conductivity (higher than the pure semiconductor or metal), which delay the recombination process. These important chemical and electrical characteristics do impart to this material certain attractiveness for potential applications such as photocatalysis.

In this study, we focused on the evaluation of the effect of graphene oxide content on the photocatalytic activity of ZnO/GO hybrid materials for the photodegradation of triclosan in solution by UV and visible light. Furthermore, we describe the mechanism of action during the degradation of TCS.

## 2. MATERIALS AND METHODS

### 2.1. MATERIALS

Zinc oxide was obtained from Degussa (Germany) under name VP AdNano ZnO 20, the graphene oxide HC (5 g/L) was purchased from Supermarket Company. Triclosan (≥97%), pure ethanol, 5.5´-dimethyl-1-pirrolidone-N-oxide (DMPO) and 2-propanol (≥99% purity) were purchased from Sigma-Aldrich. Deionised water used in the work was purified and its conductivity was 17.5 siemens.$m^{-1}$. All of the materials purchased were used as received, without any further purification.

### 2.2. METHODS

#### 2.2.1. PREPARATION OF ZnO/GO SAMPLES

ZnO/GO hybrid catalysts were prepared following the photoirradiation (FI) method previously reported [18]. The ZnO solutions (1% w/w) were prepared using isopropanol. Then, graphene oxide was added with different concentrations regarding the ZnO weight (Table 1) in order to evaluate the effect of graphene oxide in the overall photocatalytic process to degrade triclosan. The resulting ZnO/GO solutions were sonicated for one hour and after that they were exposed to UV radiation (205 nm) and mixed continuously by magnetic stirring for 2 hours. Finally, the obtained materials were recovered by centrifugation (3200 rpm for 10 minutes) and oven dried at 50°C for 12 hours, and then stored for use.

#### 2.2.2. PHOTODEGRADATION OF TRICLOSAN

The treatment of TCS was conducted by batch-type experiments. The reactor system consisted in a top open glass reactor of 150 mL capacity. The lamps for irradiation (UV or visible) were put on top of the reactor at 8 cm distance. All the mixtures were stirred for mechanical mixing. Typically, the required amount of catalyst (1 g/L) was added firstly to 100 mL of the TCS solution with an initial concentration of 8 $mgL^{-1}$ and subsequently exposed to the light illumination source over a period of 3 hours, UV light (254 nm with intensity of 858 $mW.cm^{-2}$) or visible radiation (150 W halogen lamp with

light intensity of 308 mW.cm$^{-2}$). Samples of 1 mL were withdrawn from the reactor at set intervals and filtered immediately through a 0.22 μm filter film.

The adsorption tests by the investigated photocatalysts were conducted in dark conditions; such tests were carried out before photocatalysis and it was established that adsorption takes place during the first one hour of contact between triclosan solution and photocatalyst. Thus, all the experiments began with adsorption process during one hour in dark conditions just before the photocatalytic process started.

In addition, cycling experiments were carried out to verify the photocatalyst stability. For this purpose, after each run, the catalyst was recovered, washed and reused in the subsequent run. The recovered catalysts were collected and dried to evaluate the weight loss.

As it has been by other researchers [19] the photocatalytic process using heterogeneous catalyst can be described using the Langmuir-Hinshelwood model, which was simplified to the pseudo-first order as shown in Eq. 1, was adapted to describe the photocatalytic kinetic behaviours of triclosan through the as-prepared materials.

$$ln\frac{C}{C_0} = -k_{app}t \qquad \textbf{Eq. (1)}$$

where $C$ (mg.L$^{-1}$) is the triclosan concentration at a given period of time $t$ during photodegradation, $Co$ (mg.L$^{-1}$) is the triclosan concentration at the adsorption equilibrium, $t$ (min) is the degradation time, and $k_{app}$ (min$^{-1}$) is the apparent reaction rate constant.

### 2.3. CHARACTERISATION TECHNIQUES

#### 2.3.1. SCANNING ELECTRON MICROSCOPY (SEM)

Scanning Electron Microscopy (SEM) was used to characterise the morphology and chemical composition of the ZnO/GO nanocomposites. In order to carry out the analysis, carbon membrane grids were used and over which the samples were directly deposited. A microscope FEI-FIB Dual Beam Helios Nanolab 600 was used for this purpose.

#### 2.3.2. TRANSMISSION ELECTRON MICROSCOPY (TEM)

Transmission Electron Microscopy (TEM) was used to determine the structure and morphology of the hybrid ZnO/GO compounds. For this study, a TEM Tecnai (300 keV) type FEG model (FEI Company) microscope was used with a resolution of 1.8Å point to point in HRTEM and 3Å in contrast Z, while the resolution of EDS analysis in the bright field is 20 nm and 1nm in contrast Z. The samples were supported on copper grids with carbon membrane.

#### 2.3.3. FOURIER TRANSFORM INFRARED SPECTROSCOPY (FTIR)

The equipment model Nicolet iS10 (Thermo Scientific) was used for this characterisation with measurements in the wavenumber range from 400 to 4000 cm$^{-1}$. All the analysed samples were powdered and analysed using the ATR mode.

### 2.3.4. RAMAN SPECTROSCOPY

Raman spectroscopy was used to provide an overview of the potential interaction between the pristine ZnO and GO materials in the investigated composite (ZnO/GO). The equipment InVia Microraman-Renishaw was used for this purpose using a green laser (532 nm wavelength).

### 2.3.5. ZETA POTENTIAL

This analysis was carried out using a Zetasizer Nanoseries (Malvern) in order to obtain the surface zeta potential and the average size of the synthesised samples. Solutions of $H_2SO_4$ (0.1 M) and NaOH (0.1 M) were used for this analysis.

### 2.3.6. X-RAY DIFFRACTION (XRD)

In order to determine the crystal structure of the synthesised hybrid materials and the pure ZnO and GO, the X-ray diffractmeter D8 Advance model (Bruker) was used. The conditions were at 2θ angular interval from 10 to 90 using a step size of 0.02°.

### 2.3.7. UV-VIS SPECTROSCOPY

This technique was used to determine the band gap based on absorption spectra of the ZnO and ZnO/GO photocatalysts. The equipment Cary 5000 UV-Vis-NIR with high resolution (<0.047 nm) was used in wavelength range of 190 - 3300 nm.

### 2.3.8. NITROGEN PHYSISORPTION

For this analysis, a Micromeritics TriStar II Plus analyser was used to obtain the pore dimension and surface area of the ZnO/GO hybrid catalysts and the pristine materials, ZnO and GO. All the studied materials were pre-degassed in vacuum at 120ºC for 5 h. The specific surface area was determined using the classical BET model.

### 2.3.9. HIGH PERFORMANCE LIQUID CHROMATOGRAPHY (HPLC)

The concentration of triclosan was quantified by a Shimadzu liquid chromatography equipped with UV detector. The column used was a Kinetex 5µm EVO C18 100Å, LC Column 150x4.6 mm (Phenomenex). A mobile phase consisting of 70% acetonitrile and 30% water was pumped with flow of 1 mL $min^{-1}$. The detector SPD-20AV UV wavelength was set at 254 nm. The sample was injected through auto sampler and the injection volume was 50 µL.

### 2.3.10. ELECTRO SPIN RESONANCE (ESR)

The Electro Spin Resonance (ESR) signals for radicals spin-trapped were examined using an ADANI CMS Model 8400 spectrometer, using as spin-trap reagent the 5,5´-dimethyl-1-pirrolidone-N-oxide (DMPO). In order to minimise experimental errors, the same type of quartz capillary tube was used for all the ESR measurements. The magnetic parameters of the radicals detected were obtained from direct measurements of magnetic field and microwave frequency.

## 3. RESULTS AND DISCUSSION

The results are presented and discussed according to the characterisation carried out and correlated with the photocatalytic performance of the synthesised photocatalyst.

### 3.1. PHOTOCATALYSTS CHARACTERISATION

#### 3.1.1. Electron Microscopy

Figure 1 shows SEM images of pristine zinc and graphene oxide along with the corresponding size distribution of ZnO particles obtained by zeta potential.

Figure 1-a shows different morphologies of the ZnO particles, including prisms, spheroids and tetrapods, mainly. Moreover, different particle sizes were determined, which ranged from 30 to 120 nm as it was confirmed by zeta potential (Figure 1-b). In addition, small agglomerates of ZnO particles with sizes up to 500 nm were observed.

Figures 1-c and 1-d show the images obtained by SEM for the graphene oxide sheets, with a semi-transparent continuous surface that has slight folds on it, probably as a consequence of sheet stacking.

Based on these size observations, it is suggested that obtained ZnO/GO hybrid photocatalysts are GO covered by ZnO nanoparticles and/or their agglomerates.

The following image (Figure 2-a) corresponds to ZnO/GO hybrid photocatalyst prepared by the photoirradiation method loaded with 0.25% w/w of graphene oxide.

Figure 2-a reveals the decoration on the surface of graphene oxide sheets with zinc oxide nanoparticles, which are homogeneously distributed. Zinc oxide particles exhibited the same shapes as those observed in the pure material (Figure 1-a). It must be pointed out that complete distribution of zinc oxide nanoparticles enabled the reduction of their agglomeration and enabled a good wrapped morphology of graphene sheets by ZnO particles.

The homogeneous distribution of ZnO nanoparticles on the surface of GO is probably ascribed to the photoirradiation method, since the energy used during the synthesis of hybrid photocatalysts would induce a polarity effect to ZnO, as it has been reported by Nikolai Kislov et al. in 2009 and other authors [20-22]. Thus, the polarization favours the homogeneous distribution of ZnO nanoparticles to decorate graphene oxide sheets and promotes the contact and interaction between both materials rather well, characteristically playing an important role in a photocatalytic process. The particle size of ZnO/GO hybrids synthesised in this work was between 1 and 2 μm independently of GO concentrations (0.1% w/w, 0.25% w/w or 0.5% w/w). This result was confirmed with size distribution obtained by zeta potential (Figure 2-b).

Figure 3 shows TEM images of pristine graphene oxide and the ZnO/GO hybrid photocatalyst. The observed topology, in Figure 3-a, of the GO surface is irregular and also has a clear laminate-like aggregation.

Furthermore, the approximate number of graphene layers in the analysed samples was determined, which was around 6-stacked graphene layers as shown in Figure 3-b.

Figures 3-c and 3-d display the sample TEM images of the final ZnO/GO hybrid photocatalyst compound loading with the highest concentration of graphene oxide (0.5% w/w). These images confirm the dimensions of these compounds, as determined by SEM (between 1µm and 2 µm), in addition to the information related with zinc oxide nanoparticles distribution on the graphene oxide sheets. It was corroborated the effect of photoirradiation method in the homogenous distribution of ZnO nanoparticles on graphene oxide material.

It is noteworthy that the dimensions of pure GO are higher than those present in the hybrid ZnO/GO compounds, due to the ultrasonication that was carried out during the synthesis of ZnO/GO hybrids, which reduces the GO particle size.

**3.1.2. Physisorption**

The specific area of ZnO, graphene oxide and ZnO/GO hybrid photocatalysts was determined via $N_2$ adsorption isotherms using the Brunauer Emmett Teller (BET) method.

Table 2 summarises the BET results of the surface area, pore diameter and pore volume for pristine ZnO and graphene oxide and their corresponding composites. The values of average pore diameter and pore volume were determined using the Barrett-Joyner-Halenda (BJH) method.

The results revealed that the graphene oxide showed the highest surface area for pristine materials, as it can be seen in Table 2. Among the three investigated composites, the photocatalyst loaded with 0.5% w/w of GO had the highest surface area, followed by ZnO/GO 0.25% and ZnO/GO 0.1% catalysts as it was expected. Thus, the addition of GO increases the surface area of hybrid ZnO/GO catalysts up to 57% of the initial area of zinc oxide as a consequence of good dispersion of such nanoparticles, indicating that graphene oxide is an excellent surface hybrid material to support ZnO particles. The increase in surface area is one of the most important properties of a photocatalyst to improve its efficiency.

The pore diameter values for the hybrid catalysts with values between those of base materials, ZnO (183.4 Å) and GO (682.8 Å), increasing up to 2.17 times compared with ZnO when adding a small amount of GO (0.1% w/w) and then as the GO content increases the pore diameter is reduced, and might be ascribed to the obstruction of ZnO nanoparticles surface when they interact with GO. In accordance with the last results, the pore volume varies and depends on the quantity of GO being the highest value for ZnO/GO 0.5%, then ZnO/GO 0.25% and finally ZnO/GO 0.1%, all of them present higher values than the pristine materials ZnO and GO. Such dimensions are indicative of the interaction between the ZnO and graphene oxide.

Figures 4, 5, 6 and 7 show the isotherms for pristine ZnO, ZnO/GO 0.1 %; ZnO/GO 0.25 % and ZnO/GO 0.5 %, respectively.

As it can be seen from Figures 4 to 7 Isotherms type II with H3-type hysteresis loop were obtained for all the samples, which correspond to a microstructure containing macropores or micrometric cavities in the case of ZnO/GO samples.

### 3.1.3. X-Ray Diffraction

The X-ray diffraction characterisation was used to confirm the presence of graphene oxide in the ZnO/GO hybrid photocatalysts and also to verify the possible reduction of graphene oxide during the synthesis of ZnO/GO composites under high energy (UV radiation) as previously has been reported [23-25]. Figure 8 shows the XRD patterns of pristine materials; ZnO and graphene oxide, and ZnO/GO composites synthesised in this work.

In Figure 8, it is concluded that there are no changes in the geometry observed in the diffraction directions, which are related to the size and shape of the crystal unit cell of the characterised samples, which provides information on the crystalline system studied. The ZnO pattern is identified by the characteristic peaks of the crystalline phases of hexagonal wurtzite type structure, corresponding to (100), (002), (101), (102) and (103) planes [18]. The results of the peak intensities for each analysed sample are reported in Table 3.

As can be observed from Table 3 and Figure 8, there are slight intensity changes between the patterns of the ZnO/GO hybrid photocatalysts and ZnO, in the region between 70 and 85 degrees suggesting a different position of the atoms on the surface of the crystal lattice of the ZnO due to the interactions between this compound with graphene oxide.

Regarding the diffraction pattern of GO, based on bibliographic information referring to characteristic diffraction peaks of three crystal planes of this material, the first one

corresponds to the plane 001 at 13°, the second located at 32°, which corresponds to the plane 002 and the third located at 45° for the plane 100 [26, 27].

The samples ZnO and ZnO/GO hybrid composites exhibit the typical XRD diffraction related to wurtzite structure. However, no characteristic peak of graphene oxide is observed for either ZnO/GO hybrid photocatalyst in the corresponding region, which may arise by the low content of GO in ZnO/GO hybrids.

Furthermore, the diffraction peaks of the hybrid composites are mostly unchanged compared to that of pure ZnO, which indicates that the lattice constants of ZnO have unchanged because of surface hybridisation of the carbonaceous material [28].

### 3.1.4. Fourier Transform Infrared

The FTIR spectra of pristine ZnO and GO, and ZnO/GO hybrid material (0.5% w/w) are shown in Figure 9.

Figure 9 shows the typical fingerprint groups of graphene oxide, including the hydroxyl, carboxyl and alkoxy species. The band located around 3400 $cm^{-1}$ corresponds to the stretching vibrations of the –OH group.

The band around 1711 $cm^{-1}$ corresponds to the C=O bond of carbonyls while the band located approximately at 1612 $cm^{-1}$ is attributed to the vibration of the C=C bond and, finally, the characteristic vibration band associated with alkoxy C-O stretches bond is located around 1031 $cm^{-1}$.

The band located around 699 $cm^{-1}$ corresponding to the Zn-O bond, is preserved in the spectrum of ZnO/GO composite. It is also noted that vibrations corresponding to the epoxy, carbonyl and carboxyl bonds of the GO drastically decrease or disappear; this is due to two possibilities a) low concentration of GO in ZnO/GO samples or b) indicating the reduction of GO during the synthesis of these materials.

In particular, it should be noticed that a specific adsorption band appearing at 1386 $cm^{-1}$ that has been observed only in the ZnO/GO hybrid photocatalyst. This peak could be ascribed to the vibration of the C-O bonds formed between GO and ZnO, such a hybridisation interaction between ZnO and GO with a π-conjugative 2D system that could reduce the activation of surface oxygen atoms of ZnO, by which the photocorrosion of zinc oxide could be significantly inhibited. This phenomenon has been described in a previous research about C60-ZnO composites photocatalysts [29]. Moreover, there is a shift in the C=O band located at 1711 $cm^{-1}$ that implies the hybridisation of ZnO/GO photocatalysts [30].

### 3.1.5. Raman Spectroscopy

The Raman spectra of zinc oxide, graphene oxide and ZnO/GO photocatalyst are shown in Figure 10, from which it can be seen that the pristine zinc oxide shows an intense peak at 438 $cm^{-1}$ corresponding to $E_2$ crystal mode of wurtzite structure. The D and G bands of graphene oxide were identified at 1350 $cm^{-1}$ and l593 $cm^{-1}$, respectively. The Raman-reactive G mode at 1593 $cm^{-1}$ is attributed to all $sp^2$ carbon-type structures and provides information on the in-plane vibration of $sp^2$ bonded carbon atoms while D band suggests the presence of $sp^3$ defects in the hexagonal graphitic layers [31]. The G band has been identified within the ZnO/GO samples and is related with carbon-hybridised bonds in these composites. A slightly blue shift by 9 $cm^{-1}$ in the D band of hybrid photocatalyst compared with D band of graphene oxide and a red shift in the G band of 8 $cm^{-1}$ was observed. These shifts in the Raman peak could be attributed to the chemical interaction between ZnO and graphene oxide as was suggested by FTIR.

In addition, the D/G intensities ratio is a measure of the defects in the structure of graphitic materials. Regarding the $sp^3$ and $sp^2$ hybridisations ID/IG value, in the case of pure graphene oxide is 0.93, indicating that the intensity of the G band is higher than D band which results in a lower amount of $sp^3$ defects and less structural disorder in this material.

Compared with graphene oxide (0.93), the reduction ID/IG intensity ratio for ZnO/GO 0.5% hybrid photocatalyst (ID/IG=0.91) is observed, implying a reduction of $sp^3$ defects compared with pure graphene oxide. This fact confirms the interaction between ZnO and GO given by $sp^3$ defects. The results given herein above are consistent with the results in FTIR characterisation, revealing the reestablishment of the conjugated graphene oxide network.

### 3.1.6. UV-Vis Spectroscopy

The absorption range of light plays an important role in photocatalysis. Figure 11 shows the UV-vis diffuse reflectance spectroscopy of the samples. The Band gap values of the different synthesised photocatalysts were estimated using UV Spectroscopy based on the absorption spectra collected in a wavelength range from 200 to 800 nm. The information that provides the interaction between light and the surface of the samples analysed defines their photocatalytic performance. In Figure 11, a peak in 360 nm corresponding to the absorbance of ZnO due to the optical transition of electrons from valence to conduction band can be observed. The band gap (Eg) values were estimated using the wavelength (nm) of the intersection between the slope of each curve and the Y-axis based on the following equation [18,32]

$$\boldsymbol{Eg = \frac{hc}{\lambda}} \qquad \textbf{Eq. (2)}$$

Based on this calculation, the Band Gap value for pristine ZnO was obtained, which is 3.21 eV and in the case of ZnO/GO compounds with 0.1%, 0.25% and 0.5% of GO the values obtained are 3.20 eV, 3.17 eV and 3.12 eV, respectively (Table 4

A decrement of the band gap values of ZnO hybridised materials, regarding the pristine ZnO catalyst, has the following order ZnO > ZnO/GO 0.1% > ZnO/GO 0.25% > ZnO/GO 0.5% (Table 4).

The obtained Eg values imply an increase in light absorption intensity in the visible region due to the presence of GO, which possibly enhances the anti-photocorrosion of ZnO and increases the retention time of the electrons that are promoted from the valance band to the conductive band in ZnO semiconductor.

The stronger absorption intensity in the visible region for ZnO/GO hybrid photocatalysts is a key factor for higher photocatalytic activity even at low concentrations of GO. It can also be clearly observed that hybridised ZnO with graphene oxide showed an enhanced intensity of light absorption.

Therefore, it is possible to activate ZnO/GO hybrid photocatalysts under visible light resulting in an opportunity to use these materials under such radiation, a fact that could have an impact on reducing the operating costs in water treatment systems. Regarding the method, the photoirradiation process is an easy and simple alternative to synthesise effective ZnO/GO photoactive composites with a homogeneous distribution of ZnO particles.

### 3.1.7. Zeta Potential

Finally, zinc oxide and graphene oxide were evaluated by zeta potential, before and after they were photoirradiated with UV light as they were irradiated for the synthesis of the ZnO/GO photocatalysts. This experiment was carried out in order to determine and elucidate about polarisation effect during a photoirradiation method as it has been reported [33]. It is important to mention that both samples, previously to be evaluated, were thoroughly distillate-water washed and there was no control on pH during evaluation. It is important to have in mind that zeta potential for ZnO and GO were evaluated in water solution, as they were photoirradiated using UV light, and just polarisation it was we are focused on.

The results of this experiment showed positive zeta potential values for ZnO particles, before and after being exposed to UV radiation. These values were 58.48 mV and 50.43 mV, respectively. This first result means a partial negative polarisation of the zinc oxide particles when they are exposed to UV radiation during two hours since there was a reduction of potentiometric value in comparison with the initial obtained value in the sample.

On the other hand, for the graphene oxide sample, an initial (before photoirradiation process) negative value of zeta potential (-40.61 mV) was obtained. Then, the GO sample was irradiated, and a positive value (36.35 mV) was determined.

With this result, it is inferred that the carbon material is chemically reduced when it is subjected to UV radiation, as it has been suggested by XRD and FTIR.

Based on these results, it is concluded that the photoirradiation method promotes the interaction between graphene and zinc oxide by a negative polarisation of ZnO nanoparticles as we suggested by TEM and SEM observations and, further, the electrical conductivity of these hybrid catalysts is improved by the chemical reduction of GO particles.

Both aspects improve the properties of ZnO/GO photocatalysts synthesised by the photoirradiation method and their performance during the degradation of TCS.

### 3.2. PHOTOCATALYTIC PERFORMANCE

In order to evaluate the photocatalytic performance of ZnO/GO photocatalysts, triclosan degradation experiments were conducted in batch systems, using visible light radiation (Halogen lamp, 150 W). The catalyst adsorption capacity for all the photocatalysts was determined previously in dark conditions, and it was determined that the adsorption phenomena for all the different materials takes place in one hour. Thus, after this time (1 hour), it is feasible to evaluate the TCS degradation to exclude the effect of adsorption in the photocatalytic performance of ZnO and ZnO/GO hybrid photocatalysts.

The considered "initial concentration of Triclosan" for the photocatalysis process, with the different photocatalysts, is reported in Table 5. Such "initial concentration" was obtained once the solution has been in dark during 1 h, in order to achieve the sorption equilibrium. In addition, before the sorption process takes place, the Triclosan concentration for all the solutions (with different photocatalyst type) was 8 $mgL^{-1}$, as it was mentioned in section 2.2.2., previously.

The photocatalytic activities of the ZnO/GO hybrid materials with different loading amounts of graphene oxide, using the photodegradation of triclosan as a model reaction under visible light are shown in Figure 12, including that for the photolysis process (degradation in the absence of catalyst) and for the pristine ZnO.

It is clearly noticed that all the ZnO/GO photocatalysts exhibit much higher photocatalytic activities than photolysis (which degraded just 1% of the initial concentration of TCS) and ZnO sample. The ZnO/GO 0.5% photocatalyst exhibits the maximum degradation of triclosan (45%), while the photocatalyst ZnO/GO 0.25% degraded up to 39% of the TCS. Finally, the photocatalyst synthesised with the lowest amount of GO (0.1% w/w) and the pristine ZnO catalyst exhibited degradation percentages of 35% and 32%, respectively. Thus, graphene oxide is beneficial for charge separation and increases the electrons lifetime promoted from the valance band to conductive band reducing the recombination process in ZnO catalyst. The optimal loading amount of graphene oxide in ZnO/GO hybrid photocatalysts, for the studied range, was 0.5% w/w. This percentage is much lower quantities than those that have been reported for synthesised graphene oxide composites (mainly by solvothermal synthesis), which reach up to 5% [33, 34].

This result is an important approximation to achieve a good photocatalyst to be used under visible light synthesised by the photoirradiation method, a promising, facile and friendly technique to synthesise active photocatalysts under visible and solar light radiation.

Regarding the degradation kinetics, the Figure 13 shows the TCS photodegradation apparent rate constants $k_{app}$ on ZnO/GO hybrid photocatalysts under visible light radiation. The degradation kinetic data were fitted using a pseudo-first-order equation. The introduction of graphene oxide into ZnO increased the rate constant. The photocatalytic activity follows the order ZnO/GO 0.5% > ZnO/GO 0.25% > ZnO/GO 0.1% > ZnO, while the sample ZnO/GO 0.5% shows the highest reaction rate constant of 0.0031 $min^{-1}$ followed by ZnO/GO loaded with 0.25% w/w of graphene oxide (0.0027 $min^{-1}$). Less graphene oxide leads to a decrement of photocatalytic activity up to 0.0021 $min^{-1}$, corresponding to ZnO/GO 0.1% hybrid material. Pristine ZnO showed a rate reaction constant of 0.0020 $min^{-1}$.

The kinetic rate constants of ZnO/GO 0.5% and 0.25% were 55% and 27% higher than the rate constants exhibit by ZnO, respectively.

The ZnO/GO hybrid materials are able to improve the efficiency degradation of triclosan due to the presence of GO that confirms the role of graphene oxide as an electron tramp that retains the electrons promoted from the valance to conductive band in ZnO, which is a situation that improves the generation of a higher amount of radicals, species responsible for efficiently degrading organic molecules such as TCS.

This result contributes to the development of new active photocatalysts under visible light as has been investigated and reported in several studies that have demonstrated the possibility of the photodegradation of triclosan up to 47% using photocatalysts based on rare-earth elements such as Ceria (47%) [35], metals such as Au (10% after 5 h) [36], silver [37] and Cu [38]; and others, such as MgO, $WO_3$, $TiO_2$, ZnO or GO [39].

In order to compare the photoactivity of the as-prepared ZnO/GO hybrid photocatalyst using higher irradiation, experiments were carried out under UV light (254 nm). Figure 14 shows that ZnO/GO hybrids possess improved UV light photocatalytic activity versus the commercial ZnO and without the presence of catalyst (photolysis). The result illustrates that the ZnO/GO 0.5% hybrid photocatalyst exhibits the best performance, degrading 95% of the initial concentration of TCS, while ZnO/GO 0.25% gives 89% of degradation.

Finally, the ZnO based catalyst and ZnO/GO 0.1% degraded 83% and 85%, respectively, giving the lowest photocatalytic performance. The amounts of triclosan degraded by ZnO/GO photocatalysts are slightly better than the degradation of TCS via photolysis and ZnO.

It is important to mention that such values of removal of triclosan (up to 95%) are very convenient to improve the water quality and it is very important since the conventional water treatment methods are not high enough (<95%) so that the residual triclosan is still enough to impact the environment and affect the health of living beings

The apparent rate constants for the degradation of triclosan under UV light were determined and the results are shown in Figure 15, which reveals a linear relationship between ln ($C_0/C$) and reaction time over as-prepared samples according to the pseudo-first-order kinetics plot (Figure 15-a).

The apparent reaction rate constant ($k_{app}$) values were enhanced through the introduction of graphene oxide in ZnO catalyst. The ZnO/GO 0.5% (0.0227 $min^{-1}$) exhibited the highest $k_{app}$ value among all the samples.

This result suggests the improvement of the photodegradation efficiency of the ZnO semiconductor due to the presence of graphene oxide which acts as an electron trap enhancing the photodegradation performance of ZnO/GO photocatalysts except the hybrid material with the lowest amount of GO (0.1%) which showed a slightly decrease in the slop degradation kinetic behaviour.

These results are in accordance with those obtained under visible light radiation and demonstrate the enhancement of the photoactivity of ZnO due to the presence of graphene oxide.

On the other hand, the capacity of being reused is a very important feature for photocatalyst. In order to determine the photocatalytic reusability of ZnO/GO 0.5% sample using visible and UV light radiation, four degradation cycles were carried out. After each cycle, the photocatalyst was filtered and dried thoroughly, and then fresh TCS solution was added.

In Figure 16, we can clearly see that during four cycles the photoactivity test for the degradation of TCS under visible radiation with the ZnO/GO 0.5% the efficiency is reduced up to 27% of the initial activity and under UV light, the same photocatalyst, displays a slight decrease and shows almost no deactivation.

This observation could be attributed to no degraded TCS that is adsorbed in the surface of ZnO/GO photocatalyst which reduce the efficiency of this semiconductor.

### 3.3. MECHANISTIC STUDY

Surface area, phase structure, crystallinity and separation efficiency of photogenerated charges are crucial factors for photocatalytic activity [40]. Therefore, in the as-prepared ZnO/GO hybrid samples, the enhancement of their photocatalytic activity is attributed mainly to the effective separation of the photogenerated electron-hole pairs.

In order to confirm the mechanism further, the ESR technique and trapping experiments of radicals were performed. ESR results are shown in Figures 17 and 18 under visible

light and UV radiation, respectively. The hydroxyl radicals (DMPO-•OH) and superoxide radicals (DMPO-$O_2$•$^-$) for ZnO and ZnO/GO hybrid photocatalysts in $H_2O$ (four characteristic signals) and ethanol (six signals) using visible light are observed in Figure 17.

In both cases, it is noticed that the signals for ZnO/GO hybrid materials are more pronounced than those for the ZnO pristine sample, thus accounting for the higher photocatalytic performance of ZnO/GO loaded with 0.5% w/w of graphene oxide than the bare ZnO photocatalyst towards the degradation of triclosan.

Thus, the enhanced photocatalytic activity of ZnO/GO, at any composition, but especially 0.5% compared with pure ZnO, is due to the introduction of graphene oxide, which promotes an increase in charge separation to effective utilisation of electrons to stabilize the •OH and $O_2$•$^-$ radicals. In this case, the signals of •OH (Figure 17-a) radicals are stronger than those for $O_2$•$^-$ (Figure 17-b), which suggest the predominance of oxidative reactions whose holes are responsible for the degradation of triclosan.

Furthermore, ZnO photocatalyst present visible light photocatalytic activity but generate better performance under visible light after graphene oxide hybridisation, showing that graphene oxide is responsible for the injection of an excited electron from the LUMO (Lowest Unoccupied Molecular Orbit) orbit of graphene to the CB (Conduction Band) of ZnO [36].

The introduction of the graphene oxide can possibly cause the rapid separation of electron-hole pairs during irradiation [41] prolonging the electron-hole pair lifetime and accelerating the transfer rate of electrons [42] as shown in Scheme 1.

The ESR spectra corresponding to the experiments performed in water and ethanol solvents using UV radiation are shown in Figure 18. Figure 18-a corresponds to the hydroxyl radicals generated by the analysed samples and Figure 18-b shows the superoxide radicals. The same behaviour as observed under visible light radiation, higher signals of the hydroxyl radicals than superoxide radicals, occurred in the case of UV radiation.

It is known that ZnO absorbs light to produce photogenerated electron-hole pairs. Since the valance band (VB) position of ZnO is lower than the HOMO (Highest Occupied Molecular Orbital) orbit of graphene, the photogenerated holes on ZnO could transfer easily to graphene oxide sheets via the well-developed interface.

Meanwhile, the CB position of ZnO is lower than the LUMO orbit of graphene, and the photogenerated electrons on graphene can directly inject to the CB band of ZnO, giving a more efficient charge separation and reducing the probability of recombination, and consequently, enhancing the photocatalytic activity.

As shown in Scheme 1, the high separation efficiency of photoinduced electron-hole pairs is supposed to be responsible for the enhanced UV and visible light photocatalytic

activity, resulting in an increase in the number of holes participating in the photo-oxidation process.

These electrons could easily migrate from the inner region to the surface to participate in oxidation and reduction reactions to generate radicals which are prolonged and enriched by the presence of chemical and excellent electronic structure of graphene oxide which acts as an electron tramp, thus dramatically improving the visible light activity.

The following reactions, 1 to 7, describe the proposed reaction mechanism.

$ZnO + h\nu \rightarrow ZnO + e^- h^+$ Reaction (1)

$ZnO\ (e^-) + GO \rightarrow ZnO\ (h^+) + GO\ (e^-)$ Reaction (2)

$ZnO\ (h^+) + GO\ (e) + H_2O \rightarrow ZnO + GO + \bullet OH + H^+$ Reaction (3)

$ZnO\ (h^+) + GO\ (e) + {}^-OH \rightarrow ZnO + GO + \bullet OH$ Reaction (4)

$ZnO + GO + \bullet OH + RH \rightarrow ZnO + GO + H_2O + R\bullet$ Reaction (5)

$ZnO + GO + R\bullet + O_2 \rightarrow ZnO + GO + ROO\bullet$ Reaction (6)

$ZnO + GO + ROO\bullet + O_2 \rightarrow ZnO + GO + CO_2 + H_2O$ Reaction (7)

Such reactions describe the transportation of electron-hole pairs between ZnO and graphene oxide sheets. Thus, the photocatalytic degradation of triclosan is enhanced.

## 4. CONCLUSIONS

The photoirradiation method allows a homogeneous distribution of the ZnO particles on the graphene sheets surface due to the surface polarisation of ZnO nanoparticles by the high energy (UV) used during the photocatalyst synthesis process.

There is a good interaction between the ZnO and GO through $sp^3$ hybridisations of the graphene oxide that improves the photocatalytic efficiency of ZnO/GO photocatalysts.

It is possible to degrade up to 45% of triclosan (5.1-5.6 $mg.L^{-1}$) under visible light radiation using ZnO/GO hybrid photocatalyst even loaded at low concentrations as 0.5% w/w.

GO acts as electron scavenger reducing the recombination process and promotes the charge separation in the ZnO semiconductor between the balance and conductive band that increases the generation of •OH radicals, resulting in the increase of the apparent constant rate up to 55% in ZnO/GO hybrid photocatalyst compared to the apparent rate constant of pristine ZnO.

The ZnO/GO hybrid photocatalyst can be used in a cyclic way without a significant reduction of its efficiency to degrade triclosan.

## 5. ACKNOWLEDGEMENTS

The authors would like to thank the National Science and Technology Council of Mexico for the PhD fellowship to NCR (CONACYT-253175). The authors would also like to thank Gladys Labrada for the SEM analysis, Beatriz Rivera for the Raman and XRD analysis, Héctor Silva for the TEM analysis and Sidra Iftekhar for the ESR analysis. We acknowledge using the facilities of the national laboratory of LINAN at the IPICYT, México, and using the facilities of the Laboratory of Green Chemistry of the Lappeenranta University of Technology, Finland.

## 6. REFERENCES


[1] T. Colborn, F.S. Vom Saal, A.M. Soto, Developmental effects of endocrine-disrupting chemicals in wildlife and humans, Environ. Health Perspect. 101 (1993) 378–384.

[2] E. Diamanti-Kandarakis, J. P. Bourguignon, L.C. Giudice, et al. Endocrine-Disrupting Chemicals: An Endocrine Society Scientific Statement. Endocr. Rev. 30 (2009) 293-342. https://doi.org/10.1210/er.2009-0002.

[3] A. Stolz, G. Schönfelder, M. R. Schneider, Endocrine Disruptors: Adverse Health Effects Mediated by EGFR?, Trends Endocrinol. Metab. 29 (2018), 69-71. https://doi.org/10.1016/j.tem.2017.12.003

[4] S. Rafqah, P. Wong-Wah-Chung, S. Nelieu, J. Einhorn, M. Sarakha, Phototransformation of triclosan in the presence of TiO2 in aqueous suspension: Mechanistic approach, App. Catal. B: Environ. 66 (2006), 119-125. https://doi.org/10.1016/j.apcatb.2006.03.004

[5] J.M. Poyatos, M.M. Muñio, M.C. Almecija, J.C. Torres, E. Hontoria, F. Osorio, Advanced Oxidation Processes for Wastewater Treatment: State of the Art, Water Air Soil Pollut. 205 (2010) 187–204. https://doi.org/10.1007/s11270-009-0065-1

[6] M. A. Fox, M. T. Dulay, Heterogeneous photocatalysis, Chem. Rev. 93 (1993), 341-357. https://doi.org/10.1021/cr00017a016

[7] S.K. Pardeshi, A.B. Patil, Solar photocatalytic degradation of resorcinol a model endocrine disrupter in water using zinc oxide, J. Hazard. Mat. 163 (2009), 403-409. https://doi.org/10.1016/j.jhazmat.2008.06.111

[8] M. Kamaraj, K.S. Ranjith, S. Rajeshwari, R.T. Rajendra, H. A. Salam, Photocatalytic degradation of endocrine disruptor Bisphenol-A in the presence of prepared $Ce_xZn_{1-x}O$ nanocomposites under irradiation of sunlight, J. Environ. Sci. 26 (2014) 2362-2368. https://doi.org/10.1016/j.jes.2014.09.022

[9] C.J. Yu, T.Y. Kwong, Q. Luo, Z. Cai, Photocatalytic oxidation of triclosan, Chemosphere 65 (2006) 390-399. https://doi.org/10.1016/j.chemosphere.2006.02.011

[10] P. Georgiev, N. Kaneva, A. Bojinova, K. Papazova, K. Mircheva, K. Balashev, Effect of gold nanoparticles on the photocatalytic efficiency of ZnO films, Colloids Surf. A Physicochem. Eng. Asp. 460 (2014) 240-247. https://doi.org/10.1016/j.colsurfa.2014.02.004

[11] Y. Zheng, C. Chen, Y. Zhan, X. Lin, Q. Zheng, K. Wei, J. Zhu, Photocatalytic activity of Ag/ZnO heterostructure nanocatalyst: correlation between structure and property, J. Phys. Chem. C. 112 (2008) 10773-10777. https://doi.org/10.1021/jp8027275

[12] M. Hosseini-Sarvari, Z. Bazyar, Visible Light Driven Photocatalytic Cross-Coupling Reactions on Nano Pd/ZnO Photocatalyst at Room-Temperature, ChemistrySelect, 3 (2018), pp. 1898 – 1907. https://doi.org/10.1002/slct.201702219

[13] J. Shah, M. R. Jan, F. Khitab, Sonophotocatalytic Degradation of Textile dyes over Cu impregnated ZnO catalyst in Aqueous Solution, Process Saf. Environ. Prot. 116 (2018) 149-158. https://doi.org/10.1016/j.psep.2018.01.008

[14] J. Wenwen, S. Yongchen, L. Gong, X. Chen, Synthesis of Al-ZnO nanocomposite and its potential application in photocatalysis and electrochemistry, Inorg. Chem. Commun. 88 (2018) 51-55. https://doi.org/ 10.1016/j.inoche.2017.12.013
[15] J. Park, Visible and near infrared light active photocatalysis based on conjugated polymers, J. Ind. Eng, Chem. 51 (2017) 27-43. https://doi.org/ 10.1016/j.jiec.2017.03.022
[16] P.T. Kurnianditia, T. Lling-Lling, W. Ong, W. S. Chang, S. Chai, Graphene oxide: Exploiting its unique properties toward visible-light-driven photocatalysis, Appl. Mater. Today, 4 (2016) 9-16. https://doi.org/10.1016/j.apmt.2016.04.001
[17] L. Xinjuan, P. Likun, Z. Qingfei, L. Tian, Z. Guang, C. Taiqiang, L. Ting, S. Zhuo, S. Changqing, UV-assisted photocatalytic synthesis of ZnO–reduced graphene oxide composites with enhanced photocatalytic activity in reduction of Cr (VI), Chem. Eng. J. 183 (2012) 238-243. https://doi.org/10.1016/j.cej.2011.12.068
[18] A.B. Jasso-Salcedo, A.G. Palestino Escobedo, V.A. Escobar Barrios, Effect of Ag, pH, and time on the preparation of Ag-functionalized zinc oxide nanoagglomerates as photocatalysts, J. Catal. 318 (2014) 170-178. https://doi.org/ 10.1016/j.jcat.2014.06.008
[19] A.R. Khataee, M. Fathinia, S. Aber, Kinetic Modeling of Liquid Phase Photocatalysis on Supported $TiO_2$ Nanoparticles in a Rectangular Flat-Plate Photoreactor, Ind. Eng. Chem. Res. 49 (2010) 12358-12364. https://doi.org/ 10.1021/ie101997u
[20] N. Kislov, J. Lahiri, H. Verma, D.Y. Goswami, E. Stefanokos, M. Batzill, Photocatalytic Degradation of Methyl Orange over Single Crystalline ZnO: Orientation Dependence of Photoactivity and Photostability of ZnO, Lagmuir 25 (2009) 3310-3315. https://doi.org/ 10.1021/la803845f
[21] M.M Tan, K. Ji-Hee, J. MunSeok, T. Anh-Thu, S. Lee Hong, Oriented ZnO nanostructures and their application in photocatalysis, J. Lumin. 185 (2017) 17-22. https://doi.org/ 10.1016/j.jlumin.2016.12.046
[22] M. Kenji, S. Noriko, M. Toshitsugu, H. Junichi, I. Miki, H. Hajime, Surface Polarity Determination of ZnO Spherical Particles Synthesized via Solvothermal Route, Cryst. Growth Des. 9 (2009) 5014-5016. https://doi.org/10.1021/cg901216g
[23] K. Ryong, M. Parvez, K. Chhowalla, UV-reduction of graphene oxide and its application as an interfacial layer to reduce the back-transport reactions in dye-sensitized solar cells, Chem. Phys. Lett. 483 (2009) 124–127. https://doi.org/
[24] L. Guardia, S. Villar-Rodil, J.I. Paredes, R. Rozada, A. Martínez-Alonso, J.M.D. Tascón, UV light exposure of aqueous graphene oxide suspensions to promote their direct reduction, formation of graphene–metal nanoparticle hybrids and dye degradation, Carbon 50 (2012) 1014–1024. https://doi.org/ doi.org/10.1016/j.carbon.2011.10.005
[25] J. Tianhao, H. Yongyong, S. Mei, M. Nan, The mechanism of the reaction of graphite oxide to reduced graphene oxide under ultraviolet irradiation, Carbon 54 (2013) 412–418. https://doi.org/ 10.1016/j.carbon.2012.11.057
[26] L. Tian, P. Likun, L. Xinjuan, L. Ting, Z. Guang, S. Zhuo, Enhanced photocatalytic degradation of methylene blue by ZnO-reduced graphene oxide

composite synthesized via microwave-assisted reaction, J. Alloys Compd. 509 (2011) 10086-10091. https://doi.org/ doi.org/10.1016/j.jallcom.2011.08.045
[27] L. Benxia, L. Tongxuan, W. Yanfen, W. Zhoufeng, ZnO/graphene-oxide nanocomposite with remarkably enhanced visible-light-driven photocatalytic performance, J. Colloid Interface Sci. 377 (2012) 114-121. https://doi.org/ 10.1016/j.jcis.2012.03.060
[28] B. Xiaojuan, S. Changpo, L. Di, L. Xiaohong, W. Jun, W. Nanxi, C. Xiaojiao, Z. Ruilong, Z. Yongfa, Photocatalytic degradation of deoxynivalenol using graphene/ZnO hybrids in aqueous suspension, App. Catal. B: Environ. 204 (2017) 11–20. https://doi.org/ 10.1016/j.apcatb.2016.11.010
[29] F. Hongbo, X. Tongguang, Z. Shengbao, Z. Yongfa, Photocorrosion Inhibition and Enhancement of Photocatalytic Activity for ZnO via Hybridization with $C_{60}$, Environ. Sci. Technol. 42 (2008) 8064-8069. https://doi.org/ 10.1021/es801484x
[30] C. Fangyuan, A. Weijia, L. Li, L. Yinghua, C. Wenqua, Highly efficient removal of bisphenol A by a three-dimensional graphene hydrogel-AgBr@rGO exhibiting adsorption/photocatalysis synergy, App. Catal. B: Environ. 217 (2017) 65–80. https://doi.org/ 10.1016/j.apcatb.2017.05.078
[31] X. Tongguang, Z. Liwu, C. Hanyun, Z. Yongfa, Significantly enhanced photocatalytic performance of ZnO via graphene hybridization and the mechanism study, App. Catal. B: Environ. 101 (2011) 382-387. https://doi.org/ 10.1016/j.apcatb.2010.10.007
[32] R. López, R. Gómez, Ban gap energy estimation from diffuse reflectance measurements on sol-gel and commercial TiO2: a comparative study, J. Sol-Gel Sci. Technol. (2012) 6, 1-7. https://doi.org/ 10.1007/s10971-011-2582-9
[33] G. Williams, B. Seger, K. Prashant, $TiO_2$-Graphene Nanocomposites. UV-Assisted Photocatalytic Reduction of Graphene Oxide, ACS Nano 2, 7 (2008) 1487-1491. https://doi.org/ 10.1021/nn800251f
[34] H. Kai, C. Guiqiu, Z. Guangming, C. Anwei, H. Zhenzhen, S. Jiangbo, H. Tiantian, P. Min, H. Liang, Three-dimensional graphene supported catalysts for organic dyes, App. Catal. B: Environ. 228 (2018) 19–28. https://doi.org/10.1016/j.apcatb.2018.01.061
[35] J. Santiago-Morales, M.J. Gómez, S. Herrera-López, A.R. Fernández-Alba, E. García-Calvo, R. Rosal, Energy efficiency for the removal of non-polar pollutants during ultraviolet irradiation, visible light photocatalysis and ozonation of a wastewater effluent, Water Res. 47 (2013) 5546-5556. https://doi.org/ 10.1016/j.watres.2013.06.030
[36] X. Fei, C. Jinfan, S. Kalytchuk, C. Ling, S. Yiru, K. Dexin, C. Kung-Hui, H.L. Sit Patrick, T. Yang, Supported gold clusters as effective and reusable photocatalysts for the abatement of endocrine-disrupting chemicals under visible light, J. Catal. 354 (2017) 1-12. https://doi.org/10.1016/j.jcat.2017.07.027
[37] D. Yunrong, Y. Lifeng, Synthesis and photocatalytic activity of Ag–Ti–Si ternary modified α-Bi2O3 nanoporous spheres, Mater. Lett. 142 (2015) 225-228. https://doi.org/ 10.1016/j.matlet.2014.12.013

[38] J. Niu, Y. Dai, L. Yin, J. Shang, J.C. Crittenden, Photocatalytic reduction of triclosan on Au–Cu2O nanowire arrays as plasmonic photocatalysts under visible light irradiation, Phys. Chem. 17 (2015) 17421-17428. https://doi.org/ 10.1039/c5cp02244d.
[39] L. Zhao, J. Deng, P. Sun, J. Liu, Y. Ji, N. Nakada, Z. Qiao, H. Tanaka, Y. Yang, Nanomaterials for treating emerging contaminants in water by adsorption and photocatalysis: Systematic review and bibliometric analysis, Sci. Total Environ. 627 (2018) 1253-1263. https://doi.org/ 10.1016/j.scitotenv.2018.02.006
[40] X. Bai, L. Wang, Y. Zhu, Visible Photocatalytic Activity Enhancement of $ZnWO_4$ by Graphene Hybridization, ACS Catal. 2 (2012) 2769-2778. https://doi.org/ 10.1021/cs3005852
[41] L.W. Zhang, H.B. Fu, Y.F. Zhu, Efficient TiO2 Photocatalysts from Surface Hybridization of TiO2 Particles with Graphite-like Carbon, Adv. Funct. Mater, 18 (2008) 2180-2189. https://doi.org/ 10.1002/adfm.200701478
[42] Y. Zhang, Z. R. Tong, X. Fu, Y. J. Xu, TiO2 Graphene Nanocomposites for Gas Phase Photocatalytic Degradation of Volatile Aromatic Pollutant: Is TiO2 Graphene Truly Different from Other TiO2 Carbon Composite Materials?, ACS Nano 4, 12 (2010) 7303-7314. https://doi.org/ 10.1021/nn1024219

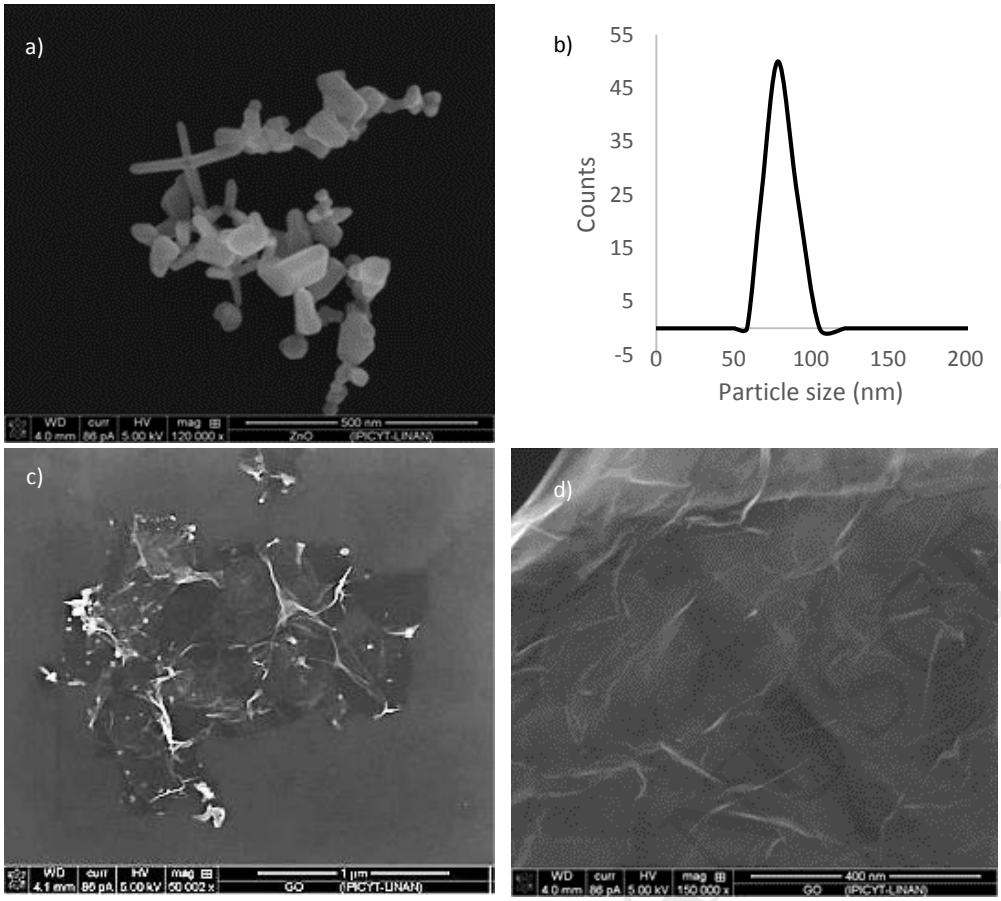


Figure 1. SEM images of a) pristine zinc oxide (120000 x), b) size distribution of pure ZnO particles obtained by zeta potential, c) pure graphene oxide (50000 x) and d) zoom of surface (150000 x).

Based on these size observations, it is suggested that obtained ZnO/GO hybrid photocatalysts are GO covered by ZnO nanoparticles and/or their agglomerates.

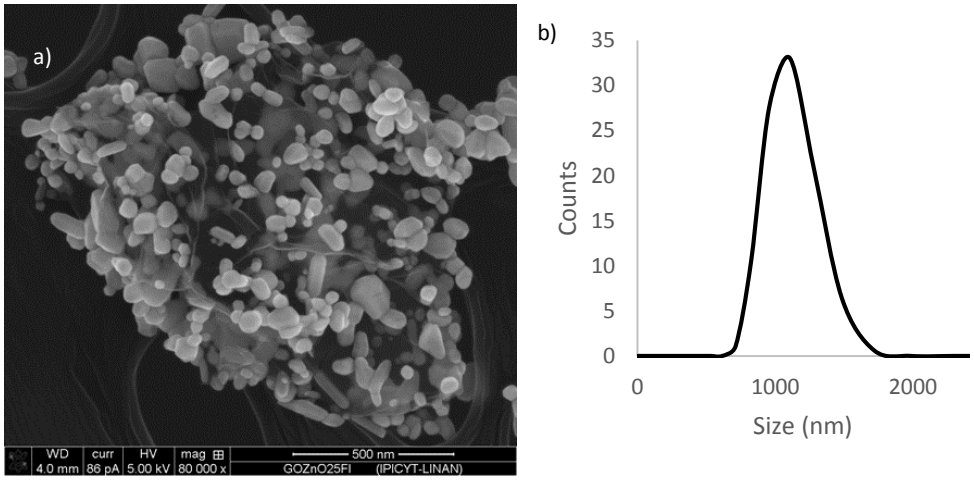


Figure 2. a) SEM images of Zn/GO hybrid material (0.25% w/w) synthesised by photoirradiation method. Magnification 80000x. b) Size distribution of ZnO/GO particles.

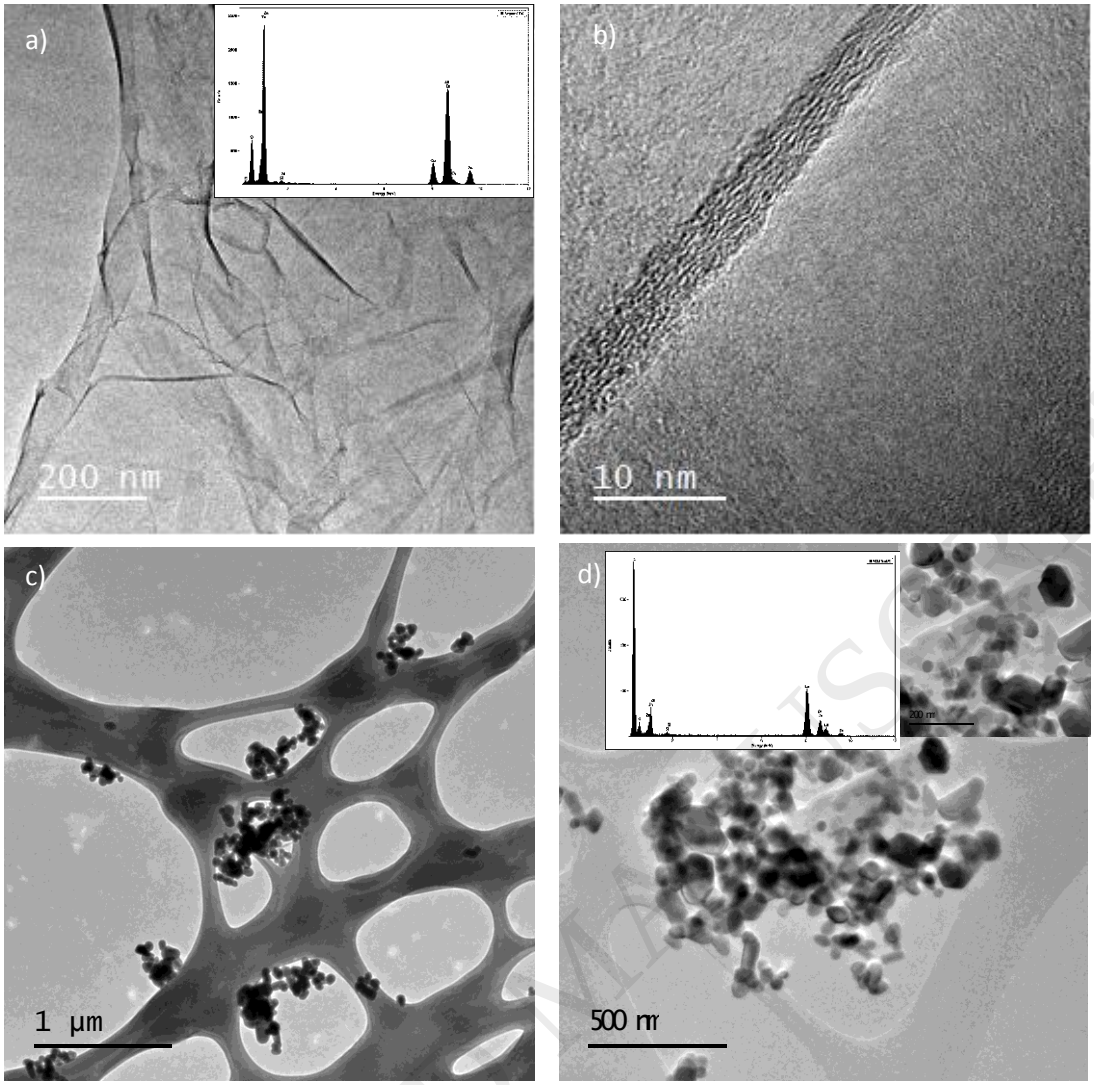


Figure 3. TEM images of a) pristine graphene oxide and b) graphene layers in GO sample c) Zn/GO photocatalysts (0.5% w/w) synthesised by the photoirradiation method with indicated scale and d) zoom of ZnO/GO photocatalyst with indicated scale (insert scale of 290 nm).

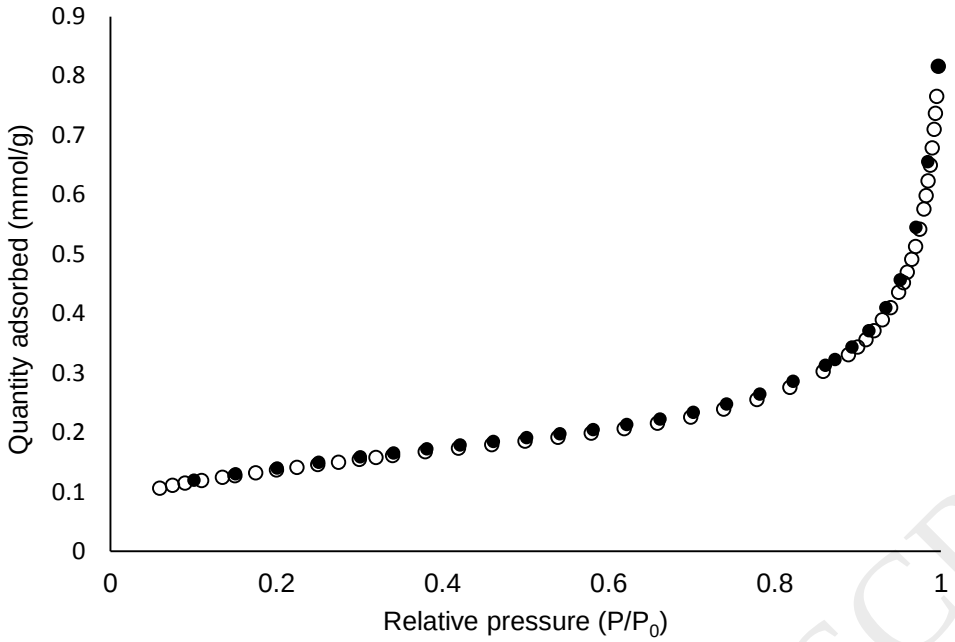


Figure 4. Physisorption isotherm for pristine ZnO.

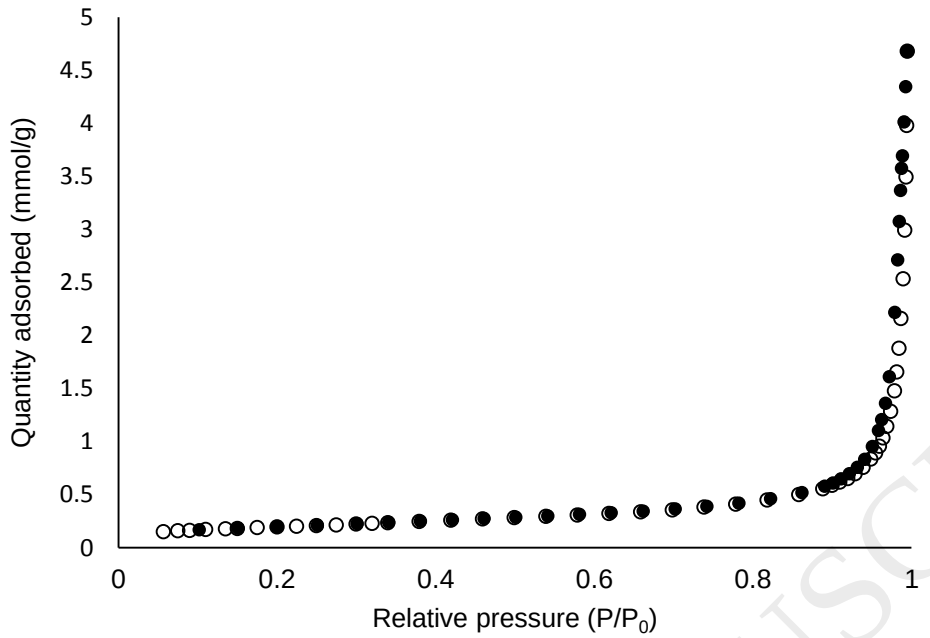


Figure 5. Physisorption isotherm for ZnO/GO 0.1 %.

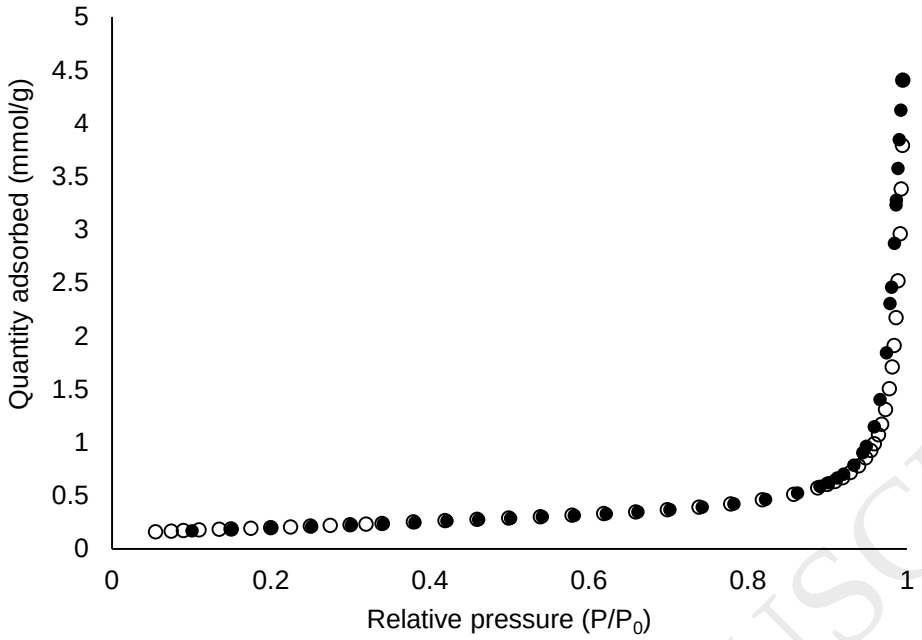


Figure 6. Physisorption isotherm for ZnO/GO 0.25 %.

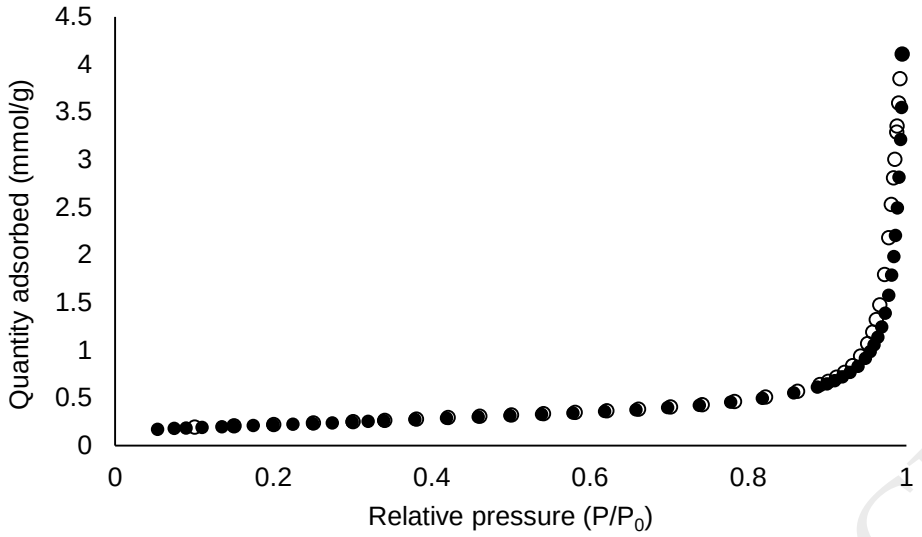


Figure 7. Physisorption isotherm for ZnO/GO 0.5 %.

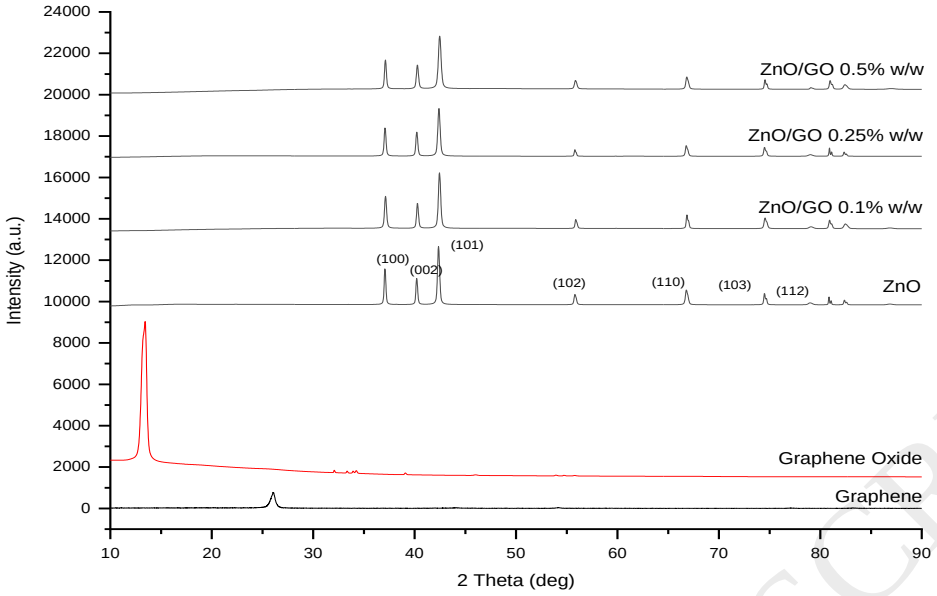


Figure 8. XRD patterns of pristine ZnO and graphene oxide; and the as-prepared ZnO/GO hybrid photocatalysts loaded with 0.1% w/w, 0.25% w/w and 0.5% w/w.

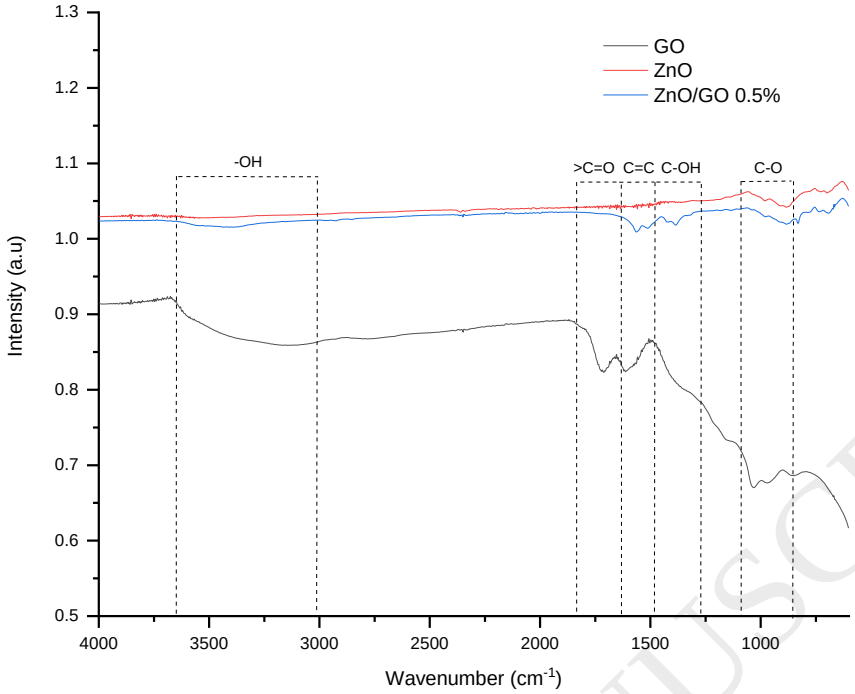


Figure 9. IR spectra of pure ZnO, pure GO and ZnO/GO nanocomposite (0.5% w/w) synthesised by the photoirradiation method.

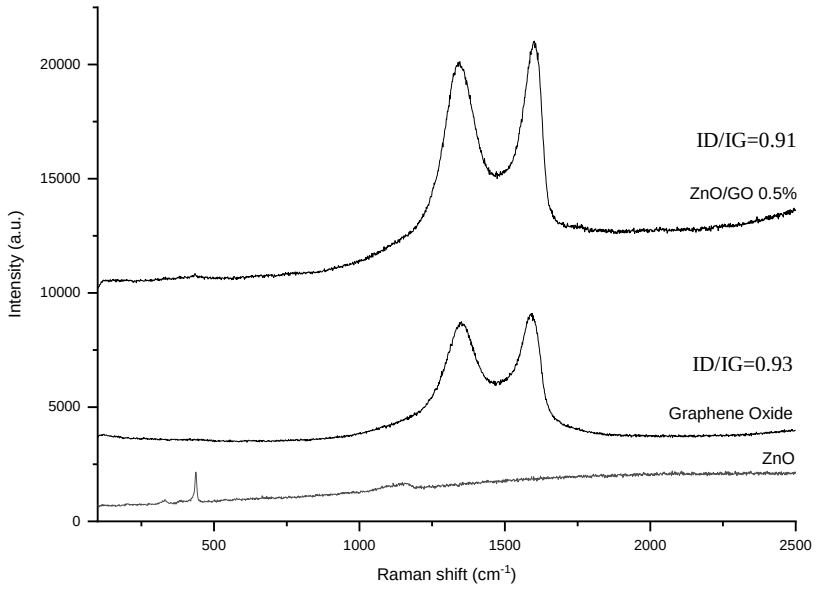


Figure 10. Raman spectra of pure ZnO, pure graphene oxide and ZnO/GO hybrid composite loaded with 0.5% w/w of graphene oxide and synthesised by the photoirradiation method.

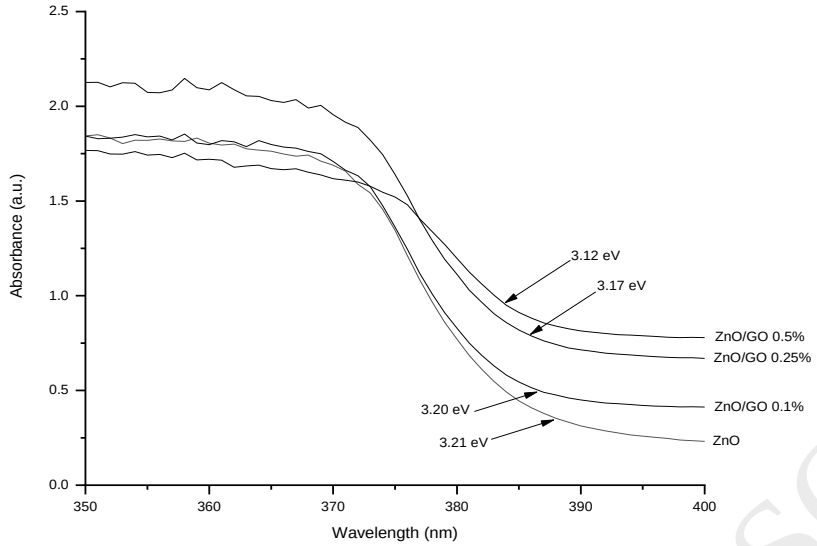


3.12 eV, respectively (Table 4)

Figure 11. UV-vis spectra of ZnO and ZnO/GO hybrids compounds with different content of GO 0.1% w/w, 0.25% w/w and 0.5% w/w.

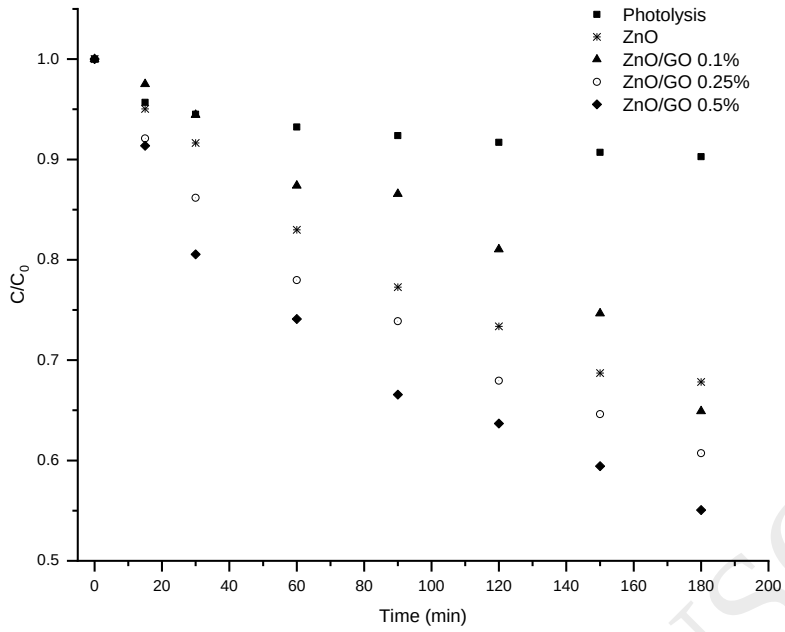


Figure 12. TCS degradation curves under visible light radiation using pristine ZnO, ZnO/GO 0.1%, ZnO/GO 0.25%, ZnO/GO 0.5% synthesised by the photoirradiation method. Conditions: pH=7, T=23°C.

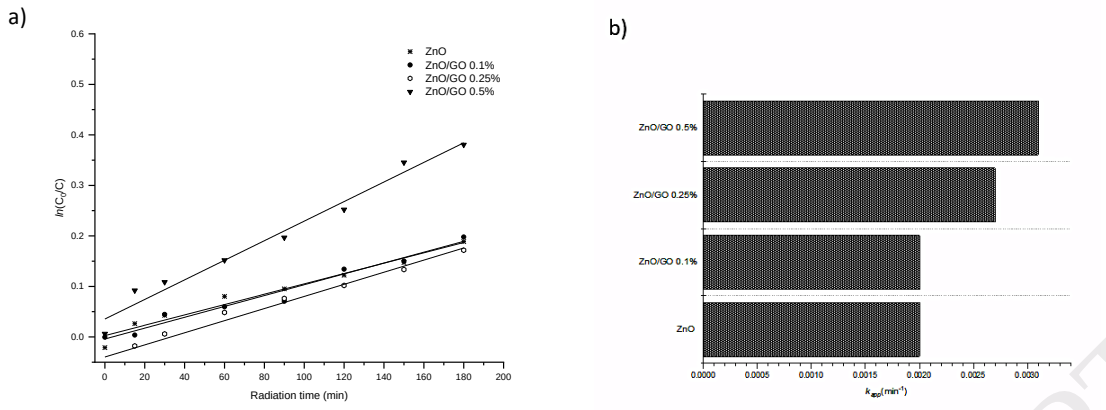


Figure 13. a) The pseudo-first-order adjustment to experimental values and b) apparent rate constants ($k_{app}$) for triclosan degradation under visible light with as-prepared samples ZnO/GO loaded with 0.5%, 0.25% and 0.1% of graphene oxide and pristine ZnO.

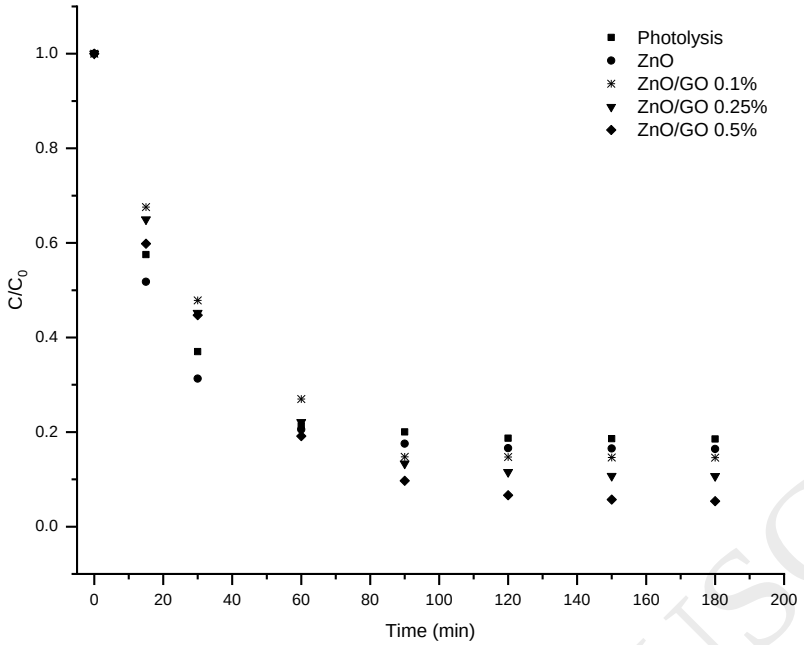


Figure 14. TCS degradation curves under UV-radiation (254nm) using pristine ZnO, ZnO/GO 0.1% w/w, ZnO/GO 0.25% w/w, ZnO/GO 0.5% w/w and in absence of catalyst (photolysis). Conditions: pH=7, T=23°C.

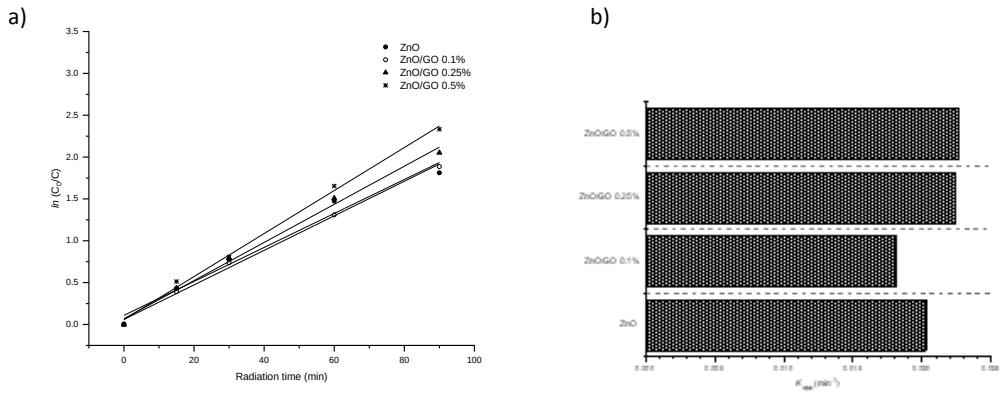


Figure 15. a) The pseudo-first-order adjustment to experimental values and b) apparent rate constants ($k_{app}$) for triclosan degradation under UV light irradiation (254 nm) with as-prepared samples ZnO/GO loaded with 0.5%, 0.25% and 0.1% of graphene oxide and pristine ZnO.

a)

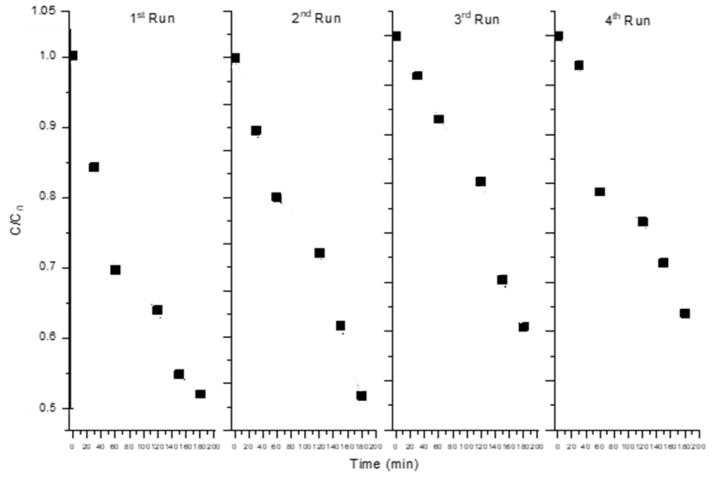


b)

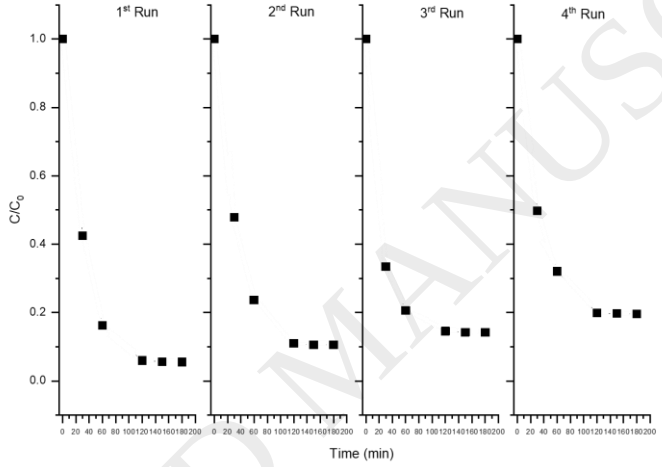


Figure 16. Cycling experiment for the photocatalytic degradation of triclosan by the prepared ZnO/GO 0.5% composite under a) visible light and b) UV radiation.

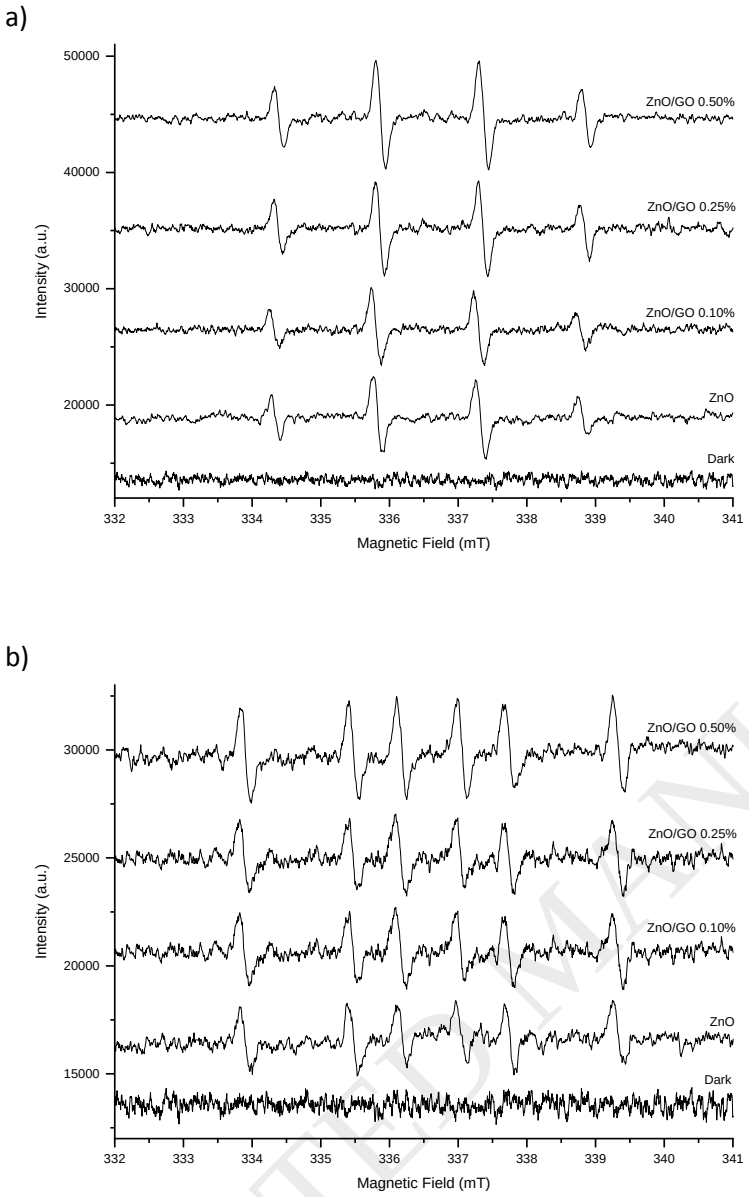


Figure 17. ESR analysis in dark conditions and visible light radiation of pristine ZnO and ZnO/GO hybrid photocatalysts in a) water and b) ethanol. DMPO was used as the radical trapper.

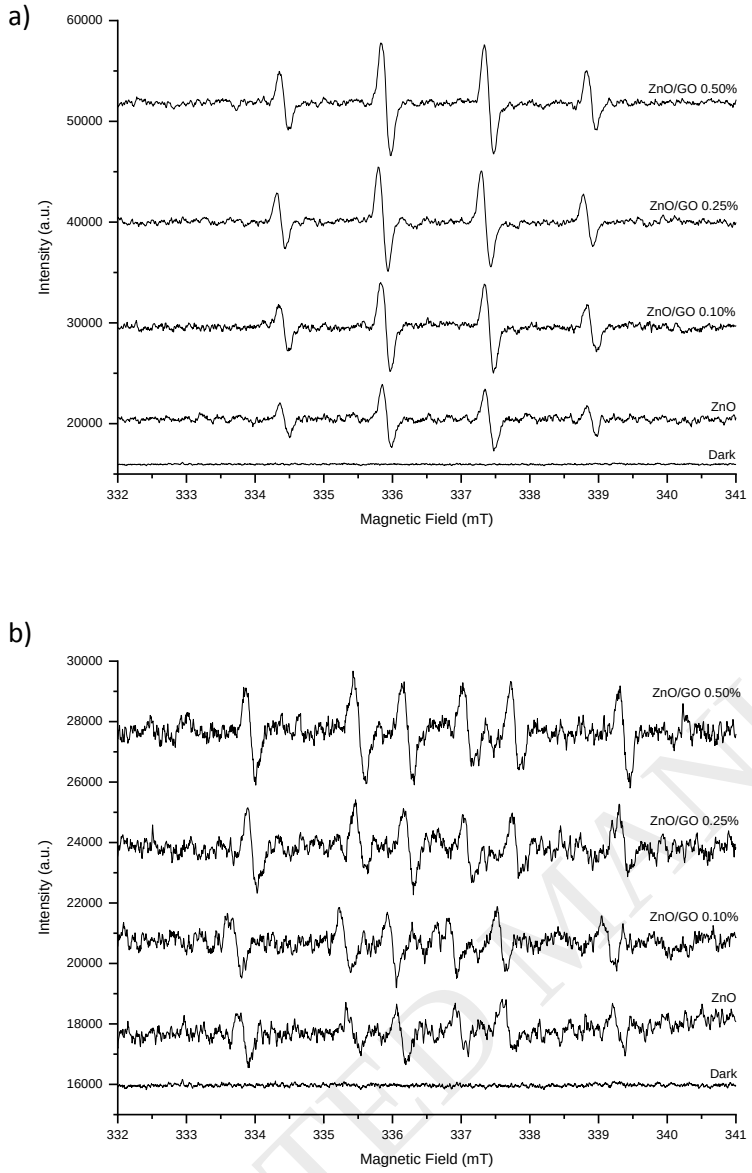


Figure 18. ESR spectra in dark conditions and UV radiation of the pure ZnO and ZnO/GO hybrid photocatalysts in a) water and b) ethanol. DMPO was used as the radical trapper.

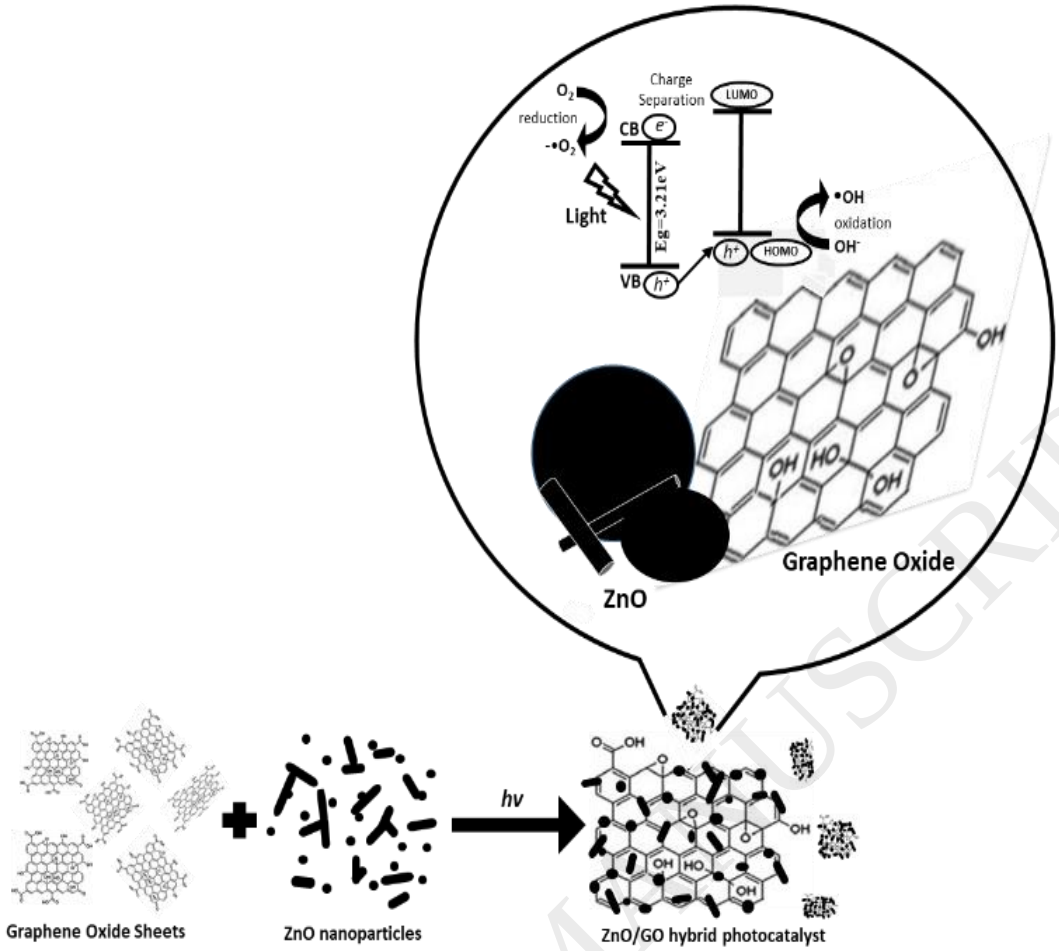


Scheme 1. Interaction of ZnO/GO hybrid photocatalyst during photocatalysis process.

Table 1. Synthesised ZnO/GO photocatalysts.

| Sample | GO Concentration (% w/w) |
|---|---|
| ZnO/GO 0.10% | 0.10 |
| ZnO/GO 0.25% | 0.25 |
| ZnO/GO 0.50% | 0.50 |

Table 2. Surface area, pore diameter and pore volume of pristine ZnO and GO materials and ZnO/GO hybrid compounds.

| Sample | BET Area ($m^2/g$) | Pore Diameter (Å) | Pore Volume ($cm^3/g$) |
|---|---|---|---|
| ZnO | 10.8 | 183.4 | 0.024 |
| GO | 46.81 | 682.8 | 0.012 |
| ZnO/GO 0.1% w/w-FI | 13.3 | 398.6 | 0.060 |
| ZnO/GO 0.25% w/w-FI | 15.8 | 306.5 | 0.073 |
| ZnO/GO 0.5% w/w-FI | 17.0 | 219.9 | 0.089 |

Table 3. Data of peak intensities corresponding to the XRD patterns of pristine ZnO and graphene oxide and ZnO/GO composites synthesised by the photoirradiation method for two hours.

| **Graphene** | | **Graphene Oxide** | | **ZnO** | |
|---|---|---|---|---|---|
| 2θ (deg) | Intensity (a. u.) | 2θ (deg) | Intensity (a. u.) | 2θ (deg) | Intensity (a. u.) |
| 26.01 | 792.6 | 13.46 | 7577.1 | 37.05 | 2219.9 |
| 43.82 | 26.8 | 32.06 | 403.12 | 40.18 | 1749.8 |
| 54.23 | 72.1 | 33.33 | 372.4 | 42.33 | 3318.1 |
| 77.70 | 37.8 | 34.22 | 359.2 | 55.79 | 986.8 |
| 83.32 | 49.4 | 39.06 | 280.4 | 66.77 | 1201.1 |
| | | 45.98 | 188.5 | 74.49 | 1035.6 |
| | | 53.91 | 171.1 | 78.95 | 571.9 |
| | | 54.71 | 162.6 | 80.85 | 864.4 |
| | | 55.75 | 153.6 | 82.37 | 718.3 |
| | | | | 86.79 | 517.8 |
| **ZnO/GO 0.1% w/w** | | **ZnO/GO 0.25% w/w** | | **ZnO/GO 0.5% w/w** | |
| 2θ (deg) | Intensity (a.u) | 2θ (deg) | Intensity (a.u) | 2θ (deg) | Intensity (a.u) |
| 37.10 | 2038.2 | 37.06 | 1825.1 | 37.10 | 1912.4 |
| 40.25 | 1684.6 | 40.19 | 1624.8 | 40.25 | 1690.6 |
| 42.42 | 3171.2 | 42.37 | 2757.2 | 42.44 | 3080.1 |
| 55.88 | 921.1 | 55.79 | 769.9 | 55.84 | 938.9 |
| 66.84 | 1148.8 | 66.77 | 975.3 | 66.82 | 1103.2 |
| 74.54 | 978.5 | 74.49 | 887.1 | 74.50 | 966.6 |
| 79.03 | 562.5 | 78.96 | 521.2 | 79.06 | 916.1 |
| 80.91 | 893.3 | 80.90 | 863.3 | 80.96 | 574.4 |
| 82.44 | 699.2 | 82.35 | 657.8 | 82.40 | 921.05 |
| 86.80 | 506.1 | | | 86.91 | 528.8 |

Table 4. Band gap of pristine ZnO photocatalyst and ZnO/GO hybrid materials with a different content of GO (0.1%, 0.25% and ZnO/GO 0.5%) obtained by UV-vis spectrophotometry.

| Photocatalyst | Band Gap (eV) | λ (nm) |
|---|---|---|
| ZnO | 3.21 | 386 |
| ZnO/GO 0.10% | 3.20 | 387 |
| ZnO/GO 0.25% | 3.17 | 385 |
| ZnO/GO 0.5% | 3.12 | 384 |

Table 5. Initial concentration for the different photocatalyst samples

| Photocatalyst | Triclosan "initial concentration" for photocatalysis process, $mgL^{-1}$ | Amount of Triclosan adsorbed by photocatalyst, before photocatalysis, mg |
|---|---|---|
| ZnO | 5.6 | 0.24 |
| ZnO/GO 0.10% | 5.4 | 0.26 |
| ZnO/GO 0.25% | 5.2 | 0.28 |
| ZnO/GO 0.5% | 5.1 | 0.29 |